International Journal of Nanomedicine

Dovepress
Taylor & Francis Group

Open Access Full Text Article

ORIGINAL RESEARCH

Chitosan Oligosaccharide-Functionalized Ruthenium-Curcumin Nanodots for Targeted Therapy of Acute Kidney Injury

Qin Yu[1], Xue-Ying Tan[2], Xian Liu[1], Hai-Bo Mao[3], Zhao-Gui Chen[4]

[1]Department of Urology, Beilun People's Hospital, Ningbo, Zhejiang, 315800, People's Republic of China; [2]College of Pharmacy, Zhejiang Pharmaceutical College, Ningbo, 315000, People's Republic of China; [3]Faculty of Materials Science and Chemical Engineering, Ningbo University, Ningbo, 315211, People's Republic of China; [4]Department of Nephrology, Beilun People's Hospital, Ningbo, Zhejiang, 315800, People's Republic of China

Correspondence: Qin Yu; Zhao-Gui Chen, Email 454699984@qq.com; a743381985@126.com

Background: Acute kidney injury (AKI) is a critical clinical syndrome with high morbidity and mortality, primarily driven by mitochondrial oxidative stress and tubular epithelial cell apoptosis. Current antioxidant therapies are limited by poor bioavailability and lack of renal specificity. To address this, we developed a dual-targeting nanomedicine based on ultrasmall chitosan oligosaccharide-functionalized ruthenium-curcumin nanodots (LMWC/Ru-Cur).

Methods: Ru-Cur coordination polymer nanodots were synthesized and subsequently coated with low-molecular-weight chitosan (LMWC). The nanoparticles were characterized for size, surface charge, stability, and antioxidant capacity. In vitro studies using HK-2 cells assessed cytocompatibility, cellular uptake, and protection against H_2O_2- or cisplatin-induced injury via measurements of viability, mitochondrial ROS, membrane potential, and apoptosis. In vivo efficacy and biodistribution were evaluated in murine models of ischemia-reperfusion- and cisplatin-induced AKI.

Results: The resulting LMWC/Ru-Cur nanodots exhibited uniform size (~7.6 nm), good aqueous stability, and potent broad-spectrum radical scavenging ability. They were efficiently internalized by renal tubular cells via megalin receptor-mediated endocytosis, leading to significantly enhanced renal accumulation. Treatment with LMWC/Ru-Cur attenuated oxidative stress, restored mitochondrial function, reduced apoptosis in injured HK-2 cells, and improved renal function (serum creatinine and blood urea nitrogen), histopathology, and inflammatory cytokine levels in both AKI models, outperforming free curcumin or unmodified Ru-Cur. The nanodots also demonstrated favorable short-term biocompatibility and in vivo biosafety.

Conclusion: LMWC/Ru-Cur nanodots represent a promising targeted nanotherapeutic strategy for AKI, integrating passive glomerular filtration with active receptor-mediated tubular delivery to effectively mitigate oxidative stress and mitochondrial damage, thereby preserving renal function. This work provides a rational design for metal-polyphenol based nanomedicines in the treatment of acute organ injury.

Keywords: acute kidney injury, reactive oxygen species, curcumin, megalin receptor, apoptosis

Introduction

Acute kidney injury (AKI) is a sudden loss of kidney function characterized by abrupt increases in serum creatinine and blood urea nitrogen.[1] As a key metabolic and excretory organ, the kidney is vulnerable to diverse insults, with ischemia–reperfusion (IR) injury and nephrotoxic drugs (eg, cisplatin) being among the most common causes.[2] The growing use of kidney transplantation and cardiac surgery has increased the incidence of AKI, posing a major clinical challenge. Although AKI was once considered reversible, 20–50% of survivors progress to chronic kidney disease (CKD), a leading precursor to end-stage renal disease (ESRD).[3] Current management is largely supportive, and there are no definitive therapies to prevent progression to CKD. Notably, approximately 36.6% of hospitalized patients with COVID-19 develop AKI, underscoring its clinical urgency.[4]

https://doi.org/10.2147/IJN.S601940
Received: 7 February 2026
Accepted: 19 June 2026
Published: 30 June 2026

Graphical Abstract

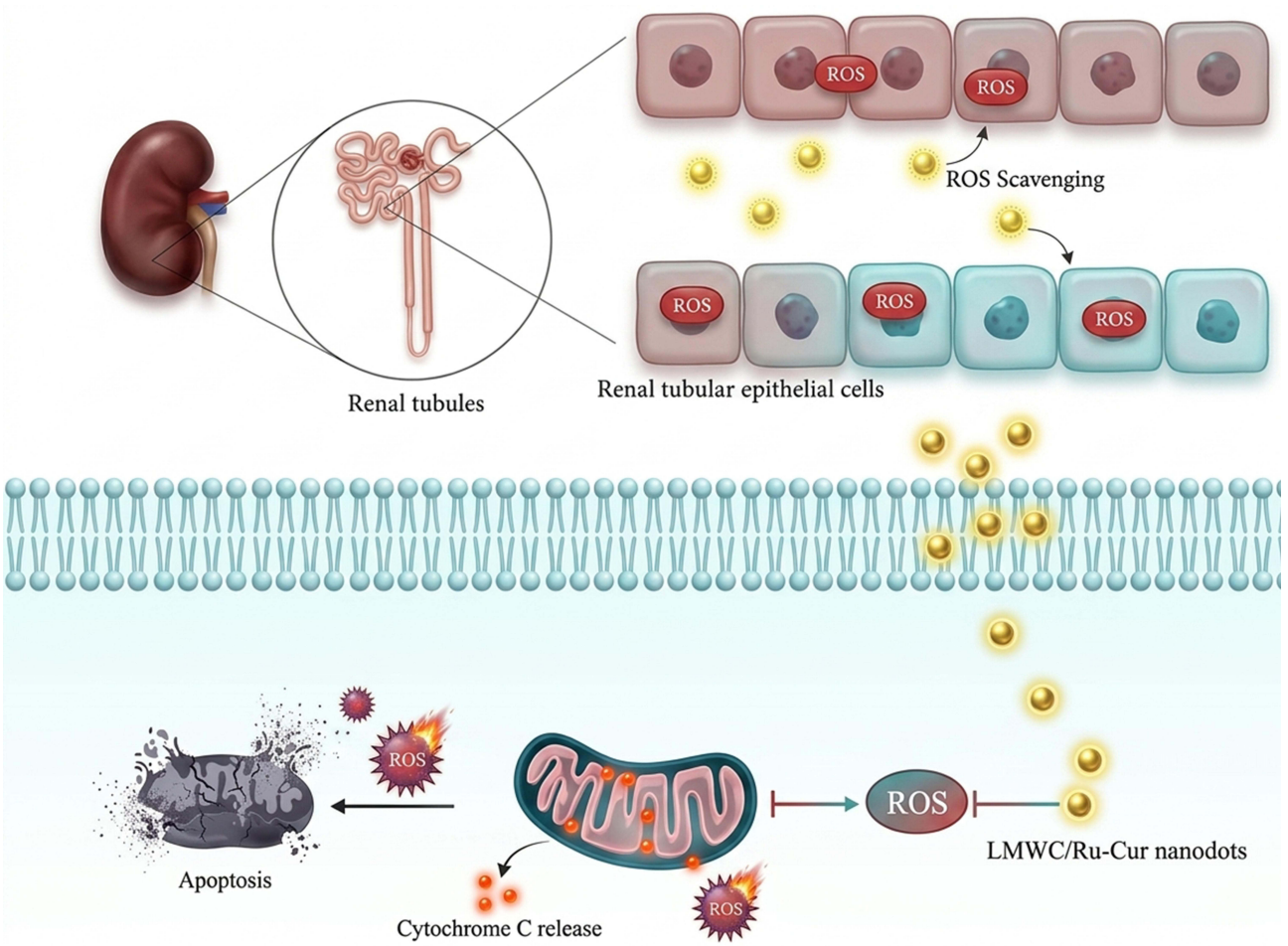

Oxidative stress driven by excessive mitochondrial reactive oxygen species (ROS), including H_2O_2, hydroxyl radicals, and superoxide, is a central mechanism of tubular epithelial cell apoptosis in AKI.[5] Although antioxidant therapy is promising, conventional agents (eg, N-acetylcysteine) suffer from poor bioavailability and off-target effects. Nanodrug delivery systems can improve renal accumulation and cellular uptake, but kidney-targeted nanomedicines face two major challenges: (1) the glomerular filtration barrier imposes stringent size requirements to enable passive renal targeting, and (2) active tubular targeting requires specific ligand–receptor interactions to avoid rapid urinary excretion.[6,7]

Building on our previous work with ultrasmall Ru/Cur nanodots,[8] we selected the metal-phenolic coordination system as the structural core because the coordination between Ru ions and curcumin (Cur) creates a stable, synergistic antioxidant framework that maximizes ROS scavenging efficiency. Specifically, the Ru-Cur core effectively solves the primary pharmacological hurdles of free Cur by significantly enhancing its water solubility and reducing its particle size to an ultrasmall range (<10 nm), which is essential for bypassing the glomerular filtration barrier. However, Ru-Cur alone faces significant targeting limitations; its net negative surface charge leads to electrostatic repulsion by the anionic glomerular basement membrane, and the absence of specific ligands results in rapid clearance rather than retention in injured tubules. To realize a "targeting upgrade", we hypothesize that functionalizing Ru/Cur with low molecular weight chitosan (LMWC) will enhance the therapeutic efficacy of the nanoparticles by enabling receptor-mediated uptake in proximal tubular epithelial cells.[9] This design leverages the interaction between the positively charged LMWC and the negatively charged Ru-Cur complex, forming

LMWC/Ru-Cur nanoparticles that engage Megalin receptors, which are highly expressed on proximal tubular epithelial cells, thereby facilitating active transport and targeted therapy for AKI.[9,10]

This study systematically evaluates the therapeutic potential of LMWC/Ru-Cur in AKI. The nanoparticles were characterized for size, zeta potential, morphology, and antioxidant activity. Fluorescence imaging assessed their biodistribution in renal tubular epithelial cells and in cisplatin- and ischemia-reperfusion-induced AKI models. Protective effects were evaluated in tubular epithelial cell injury models induced by H_2O_2 or cisplatin, with measurements of cell viability, kidney injury markers, oxidative stress, mitochondrial function, and apoptosis. Finally, efficacy was examined in animal models of AKI induced by bilateral renal pedicle clamping or cisplatin administration, with assessments of body weight, renal function, histopathology, inflammation, and oxidative stress.

Materials and Methods

Materials

Low molecular weight chitosan (LMWC, ≥90% deacetylation degree, molecular, weight: ~1500 Da) was purchased from Shandong Fengtai Biotechnology Co., Ltd. Ruthenium(III) chloride hydrate and curcumin (Cur) were purchased from Energy Chemical. Cisplatin was purchased from Aladdin. CCK-8, DAPI, Mitochondrial Membrane Potential Assay Kit (TMRE) and TUNEL were purchased from Beyotime Biotechnology. MitoSOX^{TM} Mitochondrial Superoxide Indicator (396/610 nm) was purchased from Invitrogen. Anti-KIM-1 (PA5-98302) antibody was purchased from Invitrogen. Anti-Cytochrome c (10993-1-AP), anti-Megalin (19700-1-AP) and anti-Bax (50599-2-Ig) antibodies were purchased from Proteintech Superoxide dismutase (SOD), and malondialdehyde (MDA) assay kits were purchased from Nanjing Jiancheng Bioengineering Institute. TNF-α, and IL-6 enzyme-linked immunosorbent assay (ELISA) kits were purchased from BOSTER Biological Technology. Human renal cortical proximal convoluted tubule epithelial cell (HK-2) was purchased from Procell.

Preparation and Physicochemical Characterization of LMWC/Ru-Cur Nanodots

Ru-Cur was first prepared by combining curcumin (Cur) with a ruthenium salt under stirring at room temperature as our previous study.[8] Briefly, a methanol solution (1 mL) containing 20 mg ruthenium(III) chloride hydrate was added dropwise to 5 mL of methanol under constant stirring. Subsequently, a methanol solution (1 mL) containing 10 mg Cur was introduced dropwise, and the mixture was stirred for an additional 3 h (Figure 1A). The product was purified by dialysis (MWCO: 3.5 kDa) against water overnight and stored at 4 °C until use. Fourier transform infrared (FT-IR) spectra were recorded on a Thermo Nicolet 6700 spectrometer using KBr pellets. For sample preparation, 1–2 mg of Cur or Ru–Cur was thoroughly mixed with dry KBr, placed in a die, and pressed into a transparent pellet with a hydraulic press.

To construct LMWC/Ru–Cur, 50 mg of LMWC was added to the Ru–Cur dispersion and stirred for 24 h. The mixture was then subjected to high-speed centrifugation (12,000 rpm, 20 min) to remove insoluble impurities and large LMWC aggregates. The resulting supernatant was collected and further purified by dialysis (MWCO: 3.5 kDa) against deionized water for 24 h to remove any remaining unbound LMWC (Figure 1A). The final product was stored at 4 °C for subsequent use. The morphology of LMWC/Ru–Cur was examined by transmission electron microscopy (TEM). A 0.1 mg/mL dispersion was prepared, and 10 μL was dropped onto a carbon-coated copper grid and air-dried. Hydrodynamic diameter was measured by dynamic light scattering (DLS). For stability assessment, LMWC/Ru-Cur was diluted to 100 μg/mL in equal volumes of deionized water, PBS, and DMEM/F12 medium, incubated at room temperature for 7 days, and photographed periodically to monitor visible precipitation.

Evaluation of in vitro Free Radical Scavenging Capacity

DPPH

The antioxidant activity of LMWC/Ru–Cur was evaluated using the DPPH assay. DPPH solution (400 μL, 0.5 mg/mL in methanol) was mixed with LMWC/Ru–Cur at 10, 20, 50, 100, or 200 μg/mL and incubated at 37 °C for 2 h, then cooled to room temperature. Absorbance was measured at 520 nm, and the radical scavenging ratio was calculated.[11]

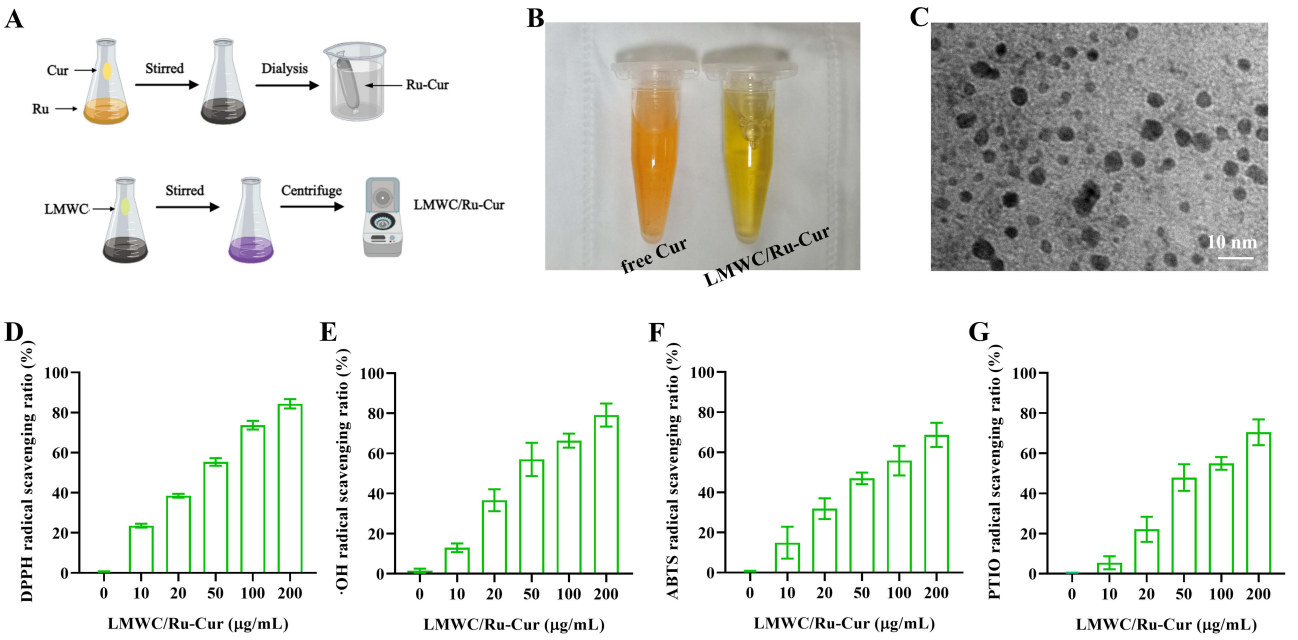

Figure 1 Characterization of the designed LMWC/Ru-Cur nanodots. (**A**) Schematic illustration of the preparation procedure of LMWC/Ru-Cur. (**B**) Photograph demonstrating the solubility of free Cur and LMWC/Ru-Cur in PBS. (**C**) Representative transmission electron microscopy (TEM) image showing the morphology of LMWC/Ru-Cur. (**D-G**) In vitro antioxidant capacity evaluations: (**D**) DPPH, (**E**) ·OH, (**F**) ABTS, and (**G**) PTIO free radicals scavenging activity at different concentrations of LMWC/Ru-Cur. Data are presented as means ± SD with n = 3 replicates per group.

ABTS

The ABTS assay kit was used to test the ability of LMWC/Ru-Cur to scavenge ABTS radicals. 400 μL of the ABTS radical working solution was incubated with the different concentrations of LMWC/Ru-Cur (10, 20, 50, 100, and 200 μg/mL). After incubation at room temperature for 2 h, the absorbance of the solution was measured at 734 nm, and the scavenging ratio was calculated.[12]

PTIO

The PTIO assay kit was used to test the ability of LMWC/Ru-Cur to scavenge PTIO radicals. 400 μL of the PTIO radical working solution (0.5 mg/mL) was incubated with the different concentrations of LMWC/Ru-Cur (10, 20, 50, 100, and 200 μg/mL). After incubation at room temperature for 2 h, the absorbance of the solution was measured at 557 nm, and the scavenging ratio was calculated.[13]

OH

The hydroxyl free radical scavenging capacity assay kit was used to test the ability of LMWC/Ru-Cur to scavenge ·OH radicals. The detection solution prepared according to the instructions was incubated with the different concentrations of LMWC/Ru-Cur (10, 20, 50, 100, and 200 μg/mL). After incubation at 37 °C for 2 h, the absorbance of the solution was measured at 510 nm, and the scavenging ratio was calculated.[14]

Cell Viability and Cytotoxicity Assessment via CCK-8 Assay

HK-2 cells were seeded in 96-well plates and incubated overnight. To assess cytocompatibility, cells were treated with LMWC/Ru-Cur at 0, 25, 50, 100, or 200 μg/mL for 24 h. Thereafter, 10 μL of CCK-8 solution was added to each well and incubated at 37 °C for 1 h in the dark. Absorbance at 450 nm was recorded to determine cell viability. Cellular morphology was imaged in parallel.

To evaluate protection against oxidative stress, HK-2 cells were exposed to 200 μM H_2O_2 for 2 h. The medium was then replaced, and cells were treated with LMWC/Ru-Cur (Cur-equivalent, 1 μg/mL) for 24 h; Cur and Ru–Cur served as controls. Cell viability was measured using CCK-8 as described above.

To assess protection against chemotherapeutic injury, HK-2 cells were incubated with 10 μM cisplatin for 12 h, followed by treatment with LMWC/Ru-Cur (Cur-equivalent, 1 μg/mL) for 24 h; Cur and Ru–Cur were used as controls. Cell viability was quantified using the CCK-8 assay.[15]

In vitro Cellular Uptake and Internalization Analysis

HK-2 cells were seeded in 96-well plates and incubated overnight. Cells were then exposed to 200 μM H_2O_2 for 2 h or 10 μM cisplatin for 12 h, followed by treatment with LMWC/Ru-Cur (Cur-equivalent, 1 μg/mL) for 2 or 6 h; Cur and Ru-Cur served as controls. After treatment, cells were washed and imaged using an inverted fluorescence microscope (Axio Observer 5, ZEISS). For flow cytometry, HK-2 cells were seeded in 6-well plates, subjected to the same treatments, and analyzed on a CytoFLEX S flow cytometer (Beckman Coulter).

Intracellular Colocalization and Receptor-Mediated Targeting Analysis

To assess Megalin-mediated endocytosis of LMWC/Ru-Cur, HK-2 cells were seeded on glass-bottom confocal dishes and incubated overnight. Cells were then treated with LMWC/Ru-Cur (Cur-equivalent, 1 μg/mL) for 2 h; Cur and Ru-Cur served as controls. Following treatment, cells were fixed in prechilled methanol (−20 °C) for 15 min. For immunofluorescence, cells were blocked with 5% BSA in PBS for 1 h, incubated with an anti-Megalin primary antibody (1:200) overnight at 4 °C, and then with an Alexa Fluor 594–conjugated secondary antibody (1:500) for 1 h. Fluorescence images were acquired using a confocal laser scanning microscope (LSM 900, Zeiss). Colocalization between Megalin (red) and the drug signal (green) was quantified in ImageJ (Coloc2) using Pearson's correlation coefficient. This approach elucidated the contribution of the LMWC shell to receptor-mediated cellular internalization.

Detection of Mitochondrial Reactive Oxygen Species (ROS) via MitoSOX Probe

MitoSOX Red is a live-cell–permeant probe that accumulates in mitochondria and, upon oxidation by superoxide, emits red fluorescence, enabling selective detection of mitochondrial superoxide. HK-2 cells were seeded in 24-well plates and incubated overnight. Cells were then exposed to 200 μM H_2O_2 for 2 h, after which the medium was replaced and cells were treated with LMWC/Ru-Cur (Cur-equivalent, 1 μg/mL) for 24 h; Cur and Ru-Cur served as controls. Subsequently, cells were incubated with MitoSOX working solution for 30 min at 37 °C in the dark, washed with PBS, and imaged using an inverted fluorescence microscope.[16] The same procedure was used to assess mitochondrial superoxide in cisplatin-treated cells (10 μM, 12 h).

Measurement of Mitochondrial Membrane Potential (MMP)

Tetramethylrhodamine ethyl ester (TMRE) is a cell-permeant, cationic fluorophore that accumulates in polarized mitochondria; loss of mitochondrial membrane potential (MMP) reduces TMRE uptake, enabling detection of MMP changes. HK-2 cells were seeded in 24-well plates and incubated overnight. Cells were then exposed to 200 μM H_2O_2 for 2 h, after which the medium was replaced and cells were treated with LMWC/Ru-Cur (Cur-equivalent, 1 μg/mL) for 24 h; Cur and Ru-Cur served as controls. Following treatment, cells were washed once with PBS and incubated with TMRE staining solution (1 mL per well) for 30 min at 37 °C in the dark. The staining solution was removed, nuclei were counterstained with DAPI, and cells were imaged using an inverted fluorescence microscope.[17] The same procedure was used to assess MMP in cisplatin-treated cells.

Immunofluorescence Staining

KIM-1 expression in cells subjected to oxidative stress or chemotherapeutic injury (as described above) was assessed by immunofluorescence. HK-2 cells were seeded on glass-bottom confocal dishes and incubated overnight. Cells were then treated with LMWC/Ru–Cur (Cur-equivalent, 1 μg/mL) for 24 h; Cur and Ru–Cur served as controls. After treatment, cells were washed with PBS and fixed with 4% paraformaldehyde, then washed again with PBS. Cells were permeabilized with 0.1% Triton X-100, washed twice, and blocked with 2% BSA in PBS for 1 h at room temperature. Next, cells were incubated with a rabbit anti–KIM-1 primary antibody overnight at 4 °C, washed with PBS, and incubated with an Alexa Fluor 594–conjugated goat anti-rabbit secondary antibody for 1 h at 37 °C. After PBS washes to remove

unbound antibody, nuclei were counterstained with DAPI. KIM-1 expression was visualized using an inverted fluorescence microscope.[18]

Western Blotting Analysis

Following the prescribed treatments, cells were harvested and lysed using RIPA buffer supplemented with protease and phosphatase inhibitors. The lysates were centrifuged at 12,000 rpm for 15 min at 4 °C to collect the supernatant, and the total protein concentration was quantified using a BCA protein assay kit. Equal amounts of protein were separated by 15% SDS-PAGE and then transferred onto PVDF membranes. After blocking with 5% non-fat milk in TBST for 1 h at room temperature, the membranes were incubated with primary antibody (anti-Bax) overnight at 4 °C. Subsequently, the membranes were incubated with corresponding HRP-conjugated secondary antibodies for 1 h. Protein bands were visualized using an enhanced chemiluminescence (ECL) system and quantified by ImageJ software, with β-actin as the internal loading control.

Establishment of Ischemia-Reperfusion and Cisplatin-Induced AKI Models

An ischemia–reperfusion–induced AKI (IR-AKI) model was established by bilateral renal artery clamping. Mice were acclimated for one week under standard housing conditions, then anesthetized by intraperitoneal injection of 10% sodium pentobarbital (0.2–0.3 mL per mouse). Dorsal hair over the kidneys was shaved, mice were positioned prone with limbs secured, and the surgical field was disinfected with povidone–iodine. The skin and subcutaneous tissue were incised, and perirenal fat was gently dissected to expose both kidneys. Renal arteries were occluded with small hemostatic clamps for 40 min while maintaining body temperature at 37.0–38.0 °C. To prevent desiccation, exposed kidneys were covered with saline-moistened, sterile gauze. After 40 min, clamps were removed to allow reperfusion, confirmed by a color change from dark red to bright red. The subcutaneous tissue and skin were sutured sequentially, avoiding additional trauma.[19] Sham-operated mice underwent the same procedure without arterial clamping and were sutured after 40 min. For the cisplatin-induced AKI model, mice received a single intraperitoneal injection of cisplatin (15 mg/kg).[20] At the end of the study, mice were euthanized by excessive CO_2 inhalation followed by cervical dislocation, in strict accordance with the American Veterinary Medical Association (AVMA) Guidelines for the Euthanasia of Animals. All efforts were made to minimize animal suffering.

In vivo Biodistribution and Renal Targeting Assessment

Balb/c mice were randomly assigned to normal control, IR-AKI, and Cis-AKI groups. IR-AKI was induced by bilateral renal artery clamping followed by reperfusion, and Cis-AKI was induced by intraperitoneal injection of cisplatin (15 mg/kg), as described above. For the IR-AKI group, LMWC/Ru–Cur (with Cur and Ru–Cur as controls; Cur dose: 2 mg/kg) was administered via the tail vein at 2 hours post-reperfusion. For the Cis-AKI group, the administration was performed at 24 hours post-cisplatin injection. At 6 h post-injection, mice were euthanized, and the heart, liver, spleen, lungs, and kidneys were rapidly harvested, rinsed with cold PBS, blotted dry, and arrayed on a black sample stage for ex vivo fluorescence imaging to assess the biodistribution and renal accumulation of LMWC/Ru-Cur.

For intrarenal localization, kidneys were processed for frozen sectioning to preserve native drug fluorescence. Immediately after harvest, tissues were embedded in optimal cutting temperature (OCT) compound, snap-frozen in liquid nitrogen–chilled isopentane, and cryosectioned at 8–10 μm. Sections were air-dried, briefly fixed in prechilled acetone (−20 °C, 10 min), rinsed with PBS, and counterstained with DAPI before mounting in antifade medium. Sectional fluorescence was imaged on an inverted fluorescence microscope, and the distribution of LMWC/Ru-Cur (Cur and Ru-Cur as controls) within renal tubules was assessed by ImageJ-based quantification of mean fluorescence intensity within tubular regions of interest.

Kidney Function

For therapeutic efficacy evaluation, a single dose of LMWC/Ru–Cur (or controls) was administered intravenously at 2 hours post-reperfusion in the IR-AKI model, and at 24 hours post-cisplatin injection in the Cis-AKI model. Blood and kidney samples were collected at 24 hours post-treatment for subsequent analysis. Blood samples were collected from the

ocular vein, and were centrifuged to separate the serum. An automated biochemical analyzer was used to measure the levels of blood urea nitrogen (BUN) and creatinine (CRE).

Histopathological Examination

After treatment, mice were euthanized to harvest kidney tissues. The kidneys were washed with PBS, blotted dry, and placed in Eppendorf tubes containing 4% paraformaldehyde for fixation. Following 24 h of fixation, the tissues were subjected to dehydration, embedding, sectioning, and hematoxylin and eosin (H&E) staining.[21]

Measurement of Oxidative Stress Biomarkers (SOD and MDA) in Renal Tissues

Kidney tissues were harvested and processed using a tissue grinder to achieve homogenization. The resulting homogenates were then subjected to centrifugation at 4000 rpm for 10 min at 4 °C to separate the supernatant. The activities of SOD and MDA were measured using the respective assay kits. The obtained data were normalized against total protein concentrations, which were determined using the BCA protein assay.[22]

Quantification of Inflammatory Cytokines via ELISA

The changes of tumor necrosis factor-alpha (TNF-α), and interleukin-6 (IL-6) in kidney tissues were examined using ELISA kits. The assay was performed according to manufacturer's instructions.[23]

In vivo Biosafety and Systemic Biocompatibility Evaluation

Hemolysis Test

Blood samples were collected from healthy Balb/c mice into heparinized tubes and centrifuged at 3000 rpm for 5 min at 4 °C to separate red blood cells (RBCs). RBCs were then resuspended in PBS to create a 2% suspension. LMWC/Ru-Cur were dissolved in the 2% RBCs suspension to achieve final LMWC/Ru-Cur concentrations of 0.25, 0.5, 1.0, and 2.0 mg/mL. PBS was used as negative control. The prepared samples were incubated in a shaking incubator at 37 °C and 75 rpm for 2 h. Subsequently, the samples were centrifuged at 3000 g for 5 min, and 200 μL of the supernatant was collected for absorbance measurement at 540 nm using a microplate reader.[24] The hemolysis rate was calculated using the following formula:

$$\text{Hemolysis rate}\,(\%) = (A_{\text{sample}} - A_{\text{negative}})/(A_{\text{positive}} - A_{\text{negative}}) \times 100\%$$

where A_{sample} was the absorbance of the sample, A_{negative} was the absorbance of the negative control, and A_{positive} was the absorbance of the positive control. Each concentration was tested in triplicate.

Complete Blood Count (CBC) Analysis

Healthy Balb/c mice were randomly divided into two groups: the control group and the LMWC/Ru-Cur group. The mice were intravenously injected with saline and LMWC/Ru-Cur (2 mg/kg), respectively. Blood samples were collected from the mice's eyeballs at day 1, 7, and 28 post-injection for CBC analysis. The parameters analyzed included red blood cells (RBC), white blood cells (WBC), platelets (PLT), lymphocytes, hemoglobin (HGB), mean corpuscular hemoglobin (MCH), and mean corpuscular hemoglobin concentration (MCHC).

Biochemical Parameters Analysis

Healthy Balb/c mice were randomly divided into two groups: the control group and the LMWC/Ru-Cur group. The mice were intravenously injected with saline and LMWC/Ru-Cur (2 mg/kg), respectively. Blood samples were collected from the mice's retro-orbital sinus at day 1, 7, and 28 post-injection. The samples were centrifuged multiple times at 3000 rpm at 4 °C to obtain serum. Liver and kidney function tests were performed, including blood urea nitrogen (BUN), creatinine (CRE), alanine aminotransferase (ALT), and aspartate aminotransferase (AST).

Histopathological examination

Healthy Balb/c mice were also randomly divided into two groups: the control group and the LMWC/Ru-Cur group. The mice were intravenously injected with saline and LMWC/Ru-Cur (2 mg/kg), and their body weights were recorded. The mice were euthanized at day 1, 7, and 21 post-injection, and major organs (heart, liver, spleen, lungs, and kidneys) were

collected. The organs were fixed in 10% neutral formalin, embedded in paraffin, and sectioned for H&E staining. The stained sections were examined under an optical microscope, and images were captured for pathological analysis.

Statistical Analysis

Quantitative data are presented as the mean ± standard deviation (SD). One-way analysis of variance (ANOVA) was conducted to identify statistical differences, with a p-value of less than 0.05 considered statistically significant. All statistical analyses were performed using GraphPad Prism 8 software.

Results

Characterization of LMWC/Ru-Cur Nanodots

Cur, dissolved in methanol, was added dropwise to a methanol solution containing ruthenium ions and stirred, resulting in a color change from yellow to dark, indicating successful coordination between the natural product and the ruthenium ions. After overnight dialysis in water to remove unreacted ions and molecules, the solution was transferred to an aqueous phase. Fourier transform infrared (FT-IR) spectroscopy was employed to confirm the coordination between Ru ions and the hydroxyl groups of Cur. FT-IR spectroscopy showed a significant decrease in the HO-C stretching vibration peak at 1150–1200 cm^{-1} in the Ru-Cur compared to Cur, suggesting successful binding of the Ru ions to the hydroxyl groups of Cur (Figure S1). The results were consistent with previous report.[8]

To further enhance the targeting activity of the Ru-Cur complex, we encapsulated it with low molecular weight chitosan (LMWC). The Ru-Cur solution was mixed with an aqueous solution of LMWC under gentle stirring, allowing LMWC to form a protective coating around the Ru-Cur complex. This encapsulation not only improved the targeting activity of the Ru-Cur but also provided additional stability to the complex. Compared with free Cur, LMWC/Ru-Cur showed the excellent water dispersibility (Figure 1B). TEM image revealed that LMWC/Ru-Cur were uniformly distributed with a size of less than 10 nm (Figure 1C). DLS results (Figure S2) showed the particle sizes of Ru-Cur and LMWC/Ru-Cur were 6.1 ± 2.2 nm and 7.6 ± 0.9 nm, respectively. The zeta potential of Ru-Cur and LMWC/Ru-Cur were −15.5 ± 0.7 mV and 4.6 ± 1.0 mV, respectively. To evaluate their stability, LMWC/Ru-Cur were incubated at 37°C for 48 h, and particle size was measured. As shown in (Figure S3), there was no significant change in particle size and no visible precipitation, indicating that LMWC/Ru-Cur exhibited good stability.

Leveraging the natural antioxidant properties of Cur, we systematically evaluated the potential of LMWC/Ru-Cur as an in vitro ROS scavenger. As shown in Figure 1D, LMWC/Ru-Cur effectively scavenged DPPH free radicals in a concentration-dependent manner, achieving 84.3% scavenging rate at 200 μg/mL. Highly reactive ·OH radicals, which can cause DNA damage, lipid peroxidation, and protein fragmentation, are considered one of the most potent types of ROS. At 200 μg/mL, LMWC/Ru-Cur was able to neutralize 79.1 ± 5.7% of ·OH radicals, demonstrating its strong scavenging capability (Figure 1E). Additionally, LMWC/Ru-Cur's ability to scavenge ABTS· and PTIO· radicals was confirmed through ABTS (Figure 1F) and PTIO (Figure 1G) assays, respectively, indicating significant antioxidant activity. These findings affirm that LMWC/Ru-Cur possesses broad-spectrum ROS scavenging abilities. In addition, comparative evaluations of radical scavenging activity were conducted across five groups: Cur, Ru, Ru-Cur, LMWC, and LMWC/Ru-Cur. Notably, Ru-Cur and LMWC/Ru-Cur exhibited comparable scavenging efficiencies (~70% at 100 μg/mL), demonstrating that LMWC surface modification did not compromise the intrinsic antioxidant activity of the Ru-Cur core (Figure S4). In contrast, free Cur showed diminished efficacy (~52% at 200 μg/mL), likely due to its poor aqueous dispersion and limited bioavailability. Neither Ru nor LMWC alone displayed detectable scavenging activity, confirming that the antioxidant function originates from the Ru-Cur rather than individual components.

The Internalization of LMWC/Ru-Cur Nanodots by Renal Tubular Epithelial Cells

HK-2 cells were selected to evaluate the impact of different concentrations of LMWC/Ru-Cur on cell viability. After incubating the cells with varying concentrations of LMWC/Ru-Cur for up to 24 h, cell viability was assessed using the CCK-8 assay. As shown in Figure S5, LMWC/Ru-Cur demonstrated good biocompatibility and low toxicity within the tested concentration range. Even at concentrations as high as 200 μg/mL, the relative cell viability remained above 90%. These

results indicated that LMWC/Ru-Cur themselves did not cause significant cytotoxic effects. In addition, no obvious changes were observed in cellular morphology of HK-2 cells treated with different concentrations of LMWC/Ru-Cur (Figure S6).

After incubated with 200 μM H_2O_2 for 2 h, HK-2 cells were further incubated with LMWC/Ru-Cur for 2 and 6 h, Cur and Ru-Cur as controls. Fluorescence imaging of HK-2 cells revealed distinct cellular uptake patterns among Cur, Ru-Cur, and LMWC/Ru-Cur (Figure 2A and B). DAPI staining (blue) marked cell nuclei, while green fluorescence indicated intracellular Cur localization. Merged images demonstrated that all three formulations successfully entered cells, with green fluorescence distributed around the nuclei. Notably, the fluorescence intensity of LMWC/Ru-Cur was significantly higher than that of free Cur and unmodified Ru-Cur, suggesting enhanced cellular internalization. This improvement likely stems from Megalin receptor-mediated endocytosis: LMWC binds to Megalin, a receptor highly expressed on renal tubular epithelial cells, thereby facilitating active uptake of the nanodrug. In contrast, free Cur and Ru-Cur, lacking LMWC modification, rely predominantly on passive diffusion, resulting in lower intracellular accumulation. Additionally, the uptake of LMWC/Ru-Cur in both normal

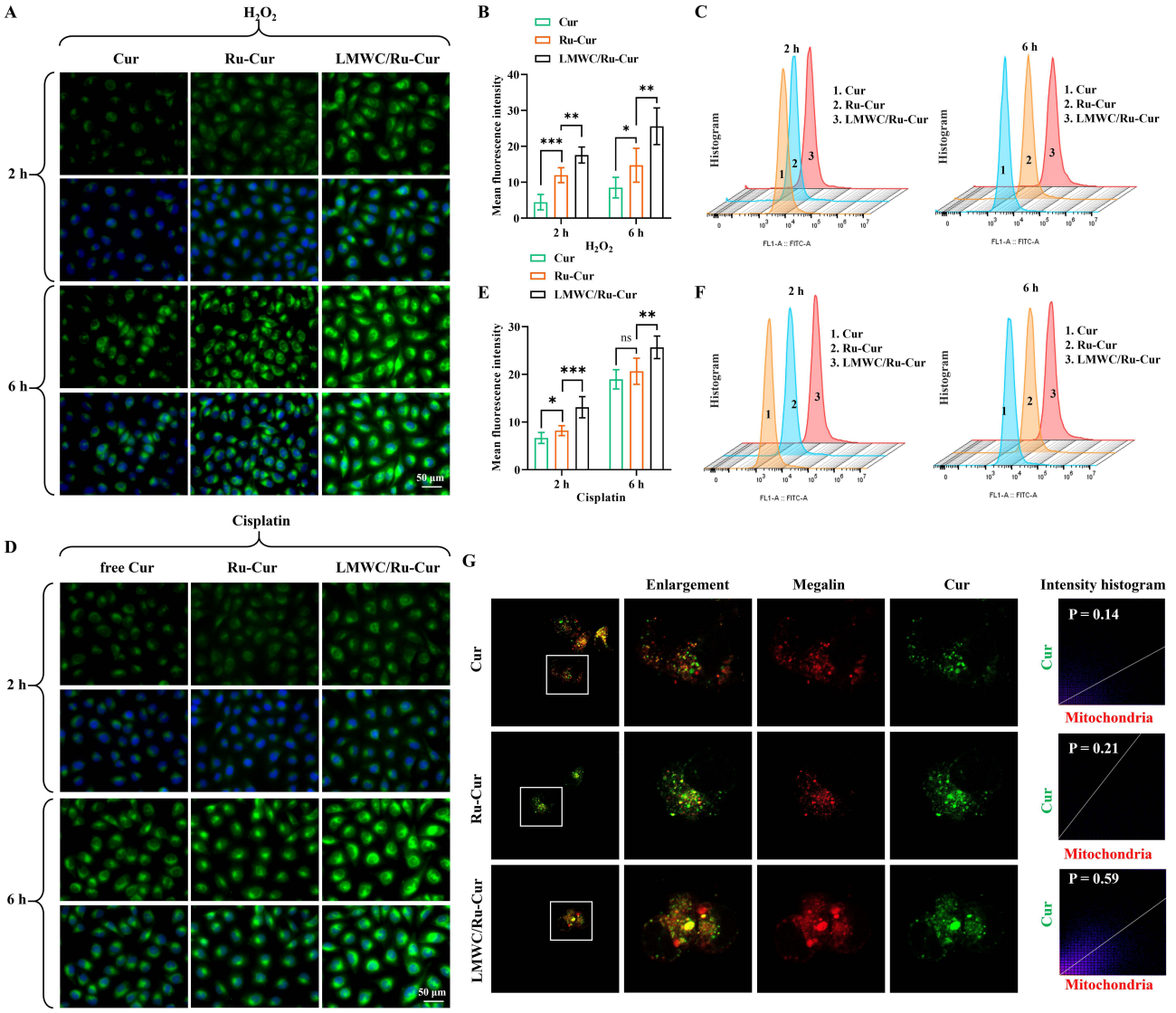

Figure 2 The cellular internalization and mitochondrial targeting of LMWC/Ru-Cur nanodots in vitro. (**A**) Representative fluorescence images and (**B**) corresponding quantitative analysis of intracellular fluorescent signals in H2O2-induced human kidney proximal tubular epithelial (HK-2) cells after incubation with Cur, Ru-Cur, or LMWC/Ru-Cur. (**C**) Flow cytometry analysis for the internalization efficiency of LMWC/Ru-Cur in H2O2-induced HK-2 cells. (**D**) Representative fluorescence images and (**E**) corresponding quantitative analysis in cisplatin (Cis)-induced HK-2 cells. Scale bar: 50 μm. (**F**) Flow cytometry analysis of the internalization in Cis-induced HK-2 cells. (**G**) Fluorescence colocalization analysis confirming the Megalin receptor-mediated endocytosis of Cur, Ru-Cur, or LMWC/Ru-Cur in HK-2 cells. Data are presented as means ± SD with n = 6 replicates per group. *p < 0.05, **p < 0.01, ***p < 0.001, and ns = not significant.

https://doi.org/10.2147/IJN.S601940

and H_2O_2-treated HK-2 cells was similar at the 2 h and 6 h time points, indicating that the Megalin receptor-mediated active transport is not affected by the cellular state (Figure S7). Flow cytometry analysis quantitatively confirmed these findings (Figure 2C), demonstrating significantly higher intracellular fluorescence intensity in the LMWC/Ru-Cur group compared to Cur and Ru-Cur, which aligns with the qualitative observations from fluorescence imaging. In addition, the similar internalized behavior of LMWC/Ru-Cur was observed in Cis-induced HK-2 cells (Figure 2D–F). This finding suggests that LMWC/Ru-Cur is also suitable for targeting and internalizing in renal tubular epithelial cells damaged by chemotherapeutic agents, further demonstrating the versatility and robustness of the Megalin receptor-mediated uptake mechanism.

The incubation with additional LMWC was found to reduce the cellular uptake of LMWC/Ru-Cur complexes in cells induced with H_2O_2. This reduction in cellular uptake was consistently observed at both the 2 h and 6 h time points (Figure S8). Specifically, in the groups where cells were co-treated with free LMWC and LMWC/Ru-Cur, the fluorescence intensity was markedly lower compared to the groups treated with LMWC/Ru-Cur alone. This suggests that free LMWC competes with LMWC/Ru-Cur for cellular uptake, likely due to the saturation or competitive inhibition of the Megalin receptors, which are implicated in the active transport of LMWC/Ru-Cur. Fluorescence colocalization analysis further revealed distinct uptake mechanisms among the tested groups. LMWC/Ru-Cur exhibited >4-fold higher colocalization efficiency with Megalin receptors compared to free Cur, and ~2.8-fold greater than unmodified Ru-Cur (Figure 2G). Notably, Ru-Cur itself showed ~1.5-fold enhanced colocalization relative to free Cur, likely attributable to its improved cellular internalization via nanoparticle-mediated transport. However, the markedly superior colocalization of LMWC/Ru-Cur underscores the critical role of LMWC in engaging Megalin-mediated endocytosis. The pronounced colocalization disparity between LMWC/Ru-Cur and its counterparts directly validates the active targeting mechanism conferred by LMWC. While Ru-Cur's modest improvement over free Cur suggests that nanoparticle formulation enhances passive uptake, the lack of Megalin-specific ligands in Ru-Cur limits its receptor engagement. In contrast, LMWC modification enables selective binding to Megalin-a receptor abundantly expressed on renal tubular epithelial cells-thereby driving receptor-dependent intracellular trafficking.

The Internalization of LMWC/Ru-Cur Nanodots in Renal Tissues

The ex vivo fluorescence imaging results demonstrated that LMWC/Ru–Cur exhibited strong fluorescence signals in the kidney tissues of all groups: sham, IR-AKI, and Cis-AKI (Figure 3A and B). This indicates a favorable renal distribution profile for LMWC/Ru–Cur. Comparatively, the renal distribution of LMWC/Ru–Cur was significantly higher than that of Ru-Cur and Cur. Specifically, the fluorescence signal of LMWC/Ru–Cur was approximately 2.3-fold higher than Ru-Cur and approximately 3.0-fold higher than Cur. Furthermore, frozen sections of organ tissues observed under a fluorescence microscope confirmed the favorable distribution of LMWC/Ru–Cur in the kidney tissues of IR-AKI (Figure 3C and D) and Cis-AKI model mice (Figure 3E and F). These observations corroborate the ex vivo imaging findings, demonstrating that LMWC/Ru–Cur is effectively localized within the renal tissues. This marked enhancement arises from Megalin receptor-mediated active targeting. LMWC binds to Megalin, a receptor abundantly expressed on renal tubular epithelial cells, driving selective uptake and prolonged renal retention. In contrast, Ru-Cur (lacking LMWC) relies on passive glomerular filtration alone, resulting in suboptimal accumulation, while free Cur suffers from rapid systemic clearance and poor solubility.

In vitro Antioxidant Activity of LMWC/Ru-Cur Nanodots

To assess the protective effects of LMWC/Ru-Cur against oxidative stress, an H_2O_2-induced injury model was established in HK-2 renal tubular epithelial cells. LMWC/Ru-Cur treatment significantly attenuated H_2O_2 (200 μM, 2 h)-mediated cytotoxicity, restoring cell viability to 84.9% compared to 44.8% in untreated controls (Figure 4A). Notably, LMWC/Ru-Cur outperformed both Cur (60.7% viability) and unmodified Ru-Cur (67.9% viability), demonstrating its superior therapeutic efficacy.

Cisplatin, a widely used chemotherapeutic agent, is highly effective in treating various cancers but also induces nephrotoxicity, primarily through oxidative stress. Cis forms DNA adducts, leading to cellular damage and mitochondrial dysfunction in renal tubular epithelial cells. This mitochondrial impairment is a key source of ROS production.[25] Cis disrupts the mitochondrial respiratory chain, causing electron leakage that reacts with oxygen to generate excessive ROS, ultimately triggering apoptosis or necrosis in the cells. Therefore, we also investigated the protective effects of LMWC/Ru-Cur against Cis-induced cell damage. As shown in Figure S9, incubation of HK-2 cells with 10 μM Cis for 12 h reduced cell viability to

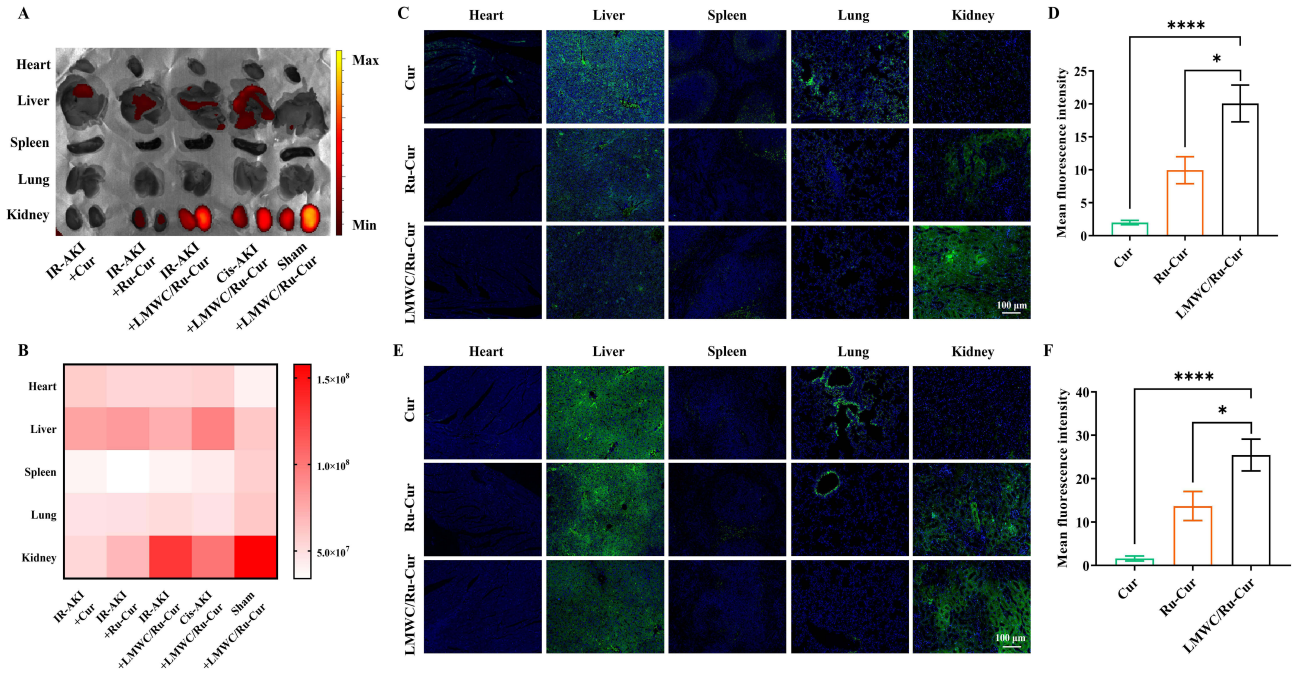

Figure 3 In vivo biodistribution and targeted renal accumulation of LMWC/Ru-Cur nanodots. (**A**) Ex vivo fluorescence imaging of major organs from ischemia-reperfusion (IR)-AKI and Cis-AKI mice at 6 h post-injection, and (**B**) corresponding quantitative analysis of the fluorescent signals. (**C**) Fluorescence imaging of tissue sections showing the biodistribution in IR-AKI mice, and (**D**) quantitative analysis of the fluorescent signals in diverse organ tissues. Scale bar: 100 μm. (**E**) Fluorescence imaging of tissue sections in Cis-AKI mice, and (**F**) quantitative analysis of the signals. Scale bar 100 μm. Data are presented as means ± SD with n = 3 replicates per group. *p < 0.05, and ****p < 0.0001.

approximately 50%, confirming the cytotoxicity induced by Cis. Cur, Ru-Cur, or LMWC/Ru-Cur treatment significantly improved cell viability compared to untreated cells. Notably, LMWC/Ru-Cur exhibited the most pronounced protective effect, further reducing the impact of Cis on cell viability compared to Cur and Ru-Cur.

Immunofluorescence staining was performed to detect the expression of kidney injury molecule-1 (KIM-1). KIM-1 is a highly sensitive biomarker for early kidney injury, with minimal expression in normal kidneys but significant upregulation upon tubular damage.[26] Compared to other kidney injury markers, KIM-1 exhibits greater specificity in tubular injury. Its increased expression during oxidative stress-induced kidney damage is often associated with elevated ROS levels and apoptosis. Therefore, measuring KIM-1 expression not only assesses the extent of tubular injury but also indirectly reflects the severity of oxidative stress. As shown in Figure 4B and C, the fluorescence intensity of KIM-1 was significantly increased in the H_2O_2-induced HK-2 cells. After treated with Cur, Ru-Cur, or LMWC/Ru-Cur, the expressions were reduced to different extent, and LMWC/Ru-Cur treatment had the best performance. In the study of Cis-induced nephrotoxicity, KIM-1 expression could also accurately reflect the damage degree of renal tubular epithelial cells. As shown in Figure S10 and S11, the fluorescence intensity of KIM-1 was significantly increased in the Cis-induced HK-2 cells. LMWC/Ru-Cur treatment effectively reduced the expression of KIM-1 compared to Cur and Ru-Cur.

In order to visually observe the scavenging behavior of mitochondrial ROS by LMWC/Ru-Cur, MitoSOX fluorescence probes were used to detect HK-2 cells. The results showed that the mitochondrial ROS levels in LMWC/Ru-Cur group were significantly lower than those in Cur group and Ru-Cur group (Figure 4D). This finding further confirmed the antioxidant capability of LMWC/Ru-Cur, effectively reducing oxidative stress-induced mitochondrial damage. Flow cytometry was used to quantitatively detect MitoSOX fluorescence intensity, and the results were consistent with the above fluorescence inverted microscope photo results (Figure 4E). Similar results were observed in Cis-induced HK-2 cells after treated with LMWC/Ru-Cur (Figure S12 and S13). It was further indicated that LMWC/Ru-Cur had a good ability to clear ROS and reduced oxidative stress damage.

Superoxide dismutase (SOD) and malondialdehyde (MDA) are critical indicators for evaluating the efficacy of antioxidants, particularly in the context of oxidative stress and related cellular damage. SOD is an essential enzyme

https://doi.org/10.2147/IJN.S601940

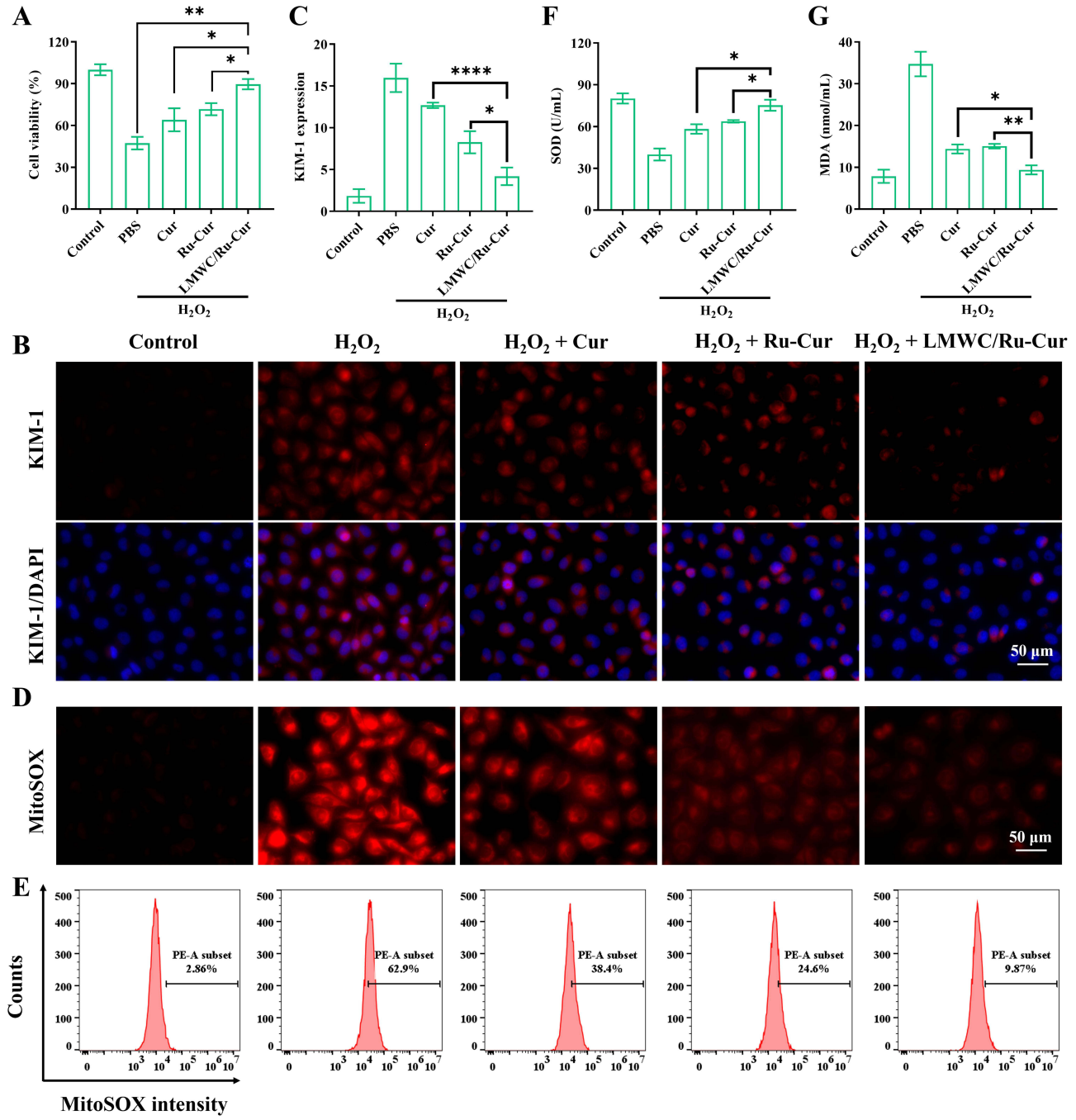

Figure 4 The in vitro antioxidant and renoprotective activities of LMWC/Ru-Cur nanodots. (**A**) Cell viability of H_2O_2-induced HK-2 cells after treated with Cur, Ru-Cur, and LMWC/Ru-Cur. (**B**) Immunofluorescence staining on the expression of kidney injury molecule-1 (KIM-1) in H_2O_2-induced HK-2 cells. Scale bar 50 μm. (**C**) Fluorescence quantitative analysis on the expression of KIM-1. (**D**) Fluorescence images of mitochondrial ROS levels in H_2O_2-induced HK-2 cells detected by MitoSOX probe. Scale bar 50 μm. (**E**) Flow cytometry results of mitochondrial ROS levels in H_2O_2-induced HK-2 cells detected by MitoSOX probe. Intracellular oxidative stress markers: (**F**) The changes of superoxide dismutase (SOD) activities and (**G**) malondialdehyde (MDA) concentrations. Data are presented as means ± SD with n = 3 replicates per group. *p < 0.05, **p < 0.01, and ****p < 0.0001.

that catalyzes the dismutation of superoxide radicals (O_2^-) into oxygen and hydrogen peroxide, thereby reducing the levels of harmful ROS within cells. An increase in SOD activity indicates an enhanced antioxidant defense, reflecting the efficacy of antioxidants in neutralizing ROS and protecting mitochondrial function. As shown in Figure 4F, the SOD activity was significantly reduced in the H_2O_2-induced HK-2 cells. After treated with Cur, Ru-Cur, or LMWC/Ru-Cur, the SOD activities were reduced to different extent, and LMWC/Ru-Cur treatment had the better performance than Cur

($P < 0.05$) or Ru-Cur ($P < 0.05$). Similarly, LMWC/Ru-Cur effectively increased the SOD activity in the Cis-induced HK-2 cells compared to Cur ($P < 0.01$) or Ru-Cur ($P < 0.05$) (Figure S14). MDA is a byproduct of lipid peroxidation, which occurs when ROS attack polyunsaturated fatty acids in cellular membranes. Elevated MDA levels are indicative of oxidative damage to cell membranes, particularly in mitochondria. As shown in Figure 4G, the MDA concentration was significantly increased in the H_2O_2-induced HK-2 cells. After treated with Cur, Ru-Cur, or LMWC/Ru-Cur, the MDA concentrations were reduced to different extent, and LMWC/Ru-Cur treatment had the better performance than Cur ($P < 0.05$) or Ru-Cur ($P < 0.01$). Similarly, LMWC/Ru-Cur effectively reduced the MDA concentrations in the Cis-induced HK-2 cells treated with Cur ($P < 0.05$) or Ru-Cur ($P < 0.05$) (Figure S15). These results showed LMWC/Ru-Cur effectively inhibited lipid peroxidation damage induced by H_2O_2 or Cis.

Excessive ROS production induced by H_2O_2 or Cis can damage mitochondrial components, including lipids, proteins, and DNA. This damage often leads to the opening of the mitochondrial permeability transition pores (mPTP), resulting in depolarization of the mitochondrial membrane and loss of mitochondrial membrane potential (MMP).[27] A decrease in MMP can impair ATP production, initiate mitochondrial dysfunction, and potentially trigger apoptosis or necrosis if the damage is severe. LMWC/Ru-Cur has been demonstrated to effectively scavenge ROS, and the next step was to further investigate the effects of LMWC/Ru-Cur on mPTP. Under normal conditions, mitochondria maintain a high negative charge, allowing the cationic probe TMRE to accumulate in the mitochondrial matrix, emitting bright orange-red fluorescence. During apoptosis, the loss of MMP leads to the sustained opening of mPTP, causing TMRE to be released into the cytoplasm and resulting in a marked decrease in mitochondrial fluorescence intensity. As shown in Figure 5A and B, the TMRE fluorescence intensity was reduced in the H_2O_2-induced HK-2 cells, and LMWC/Ru-Cur treatment effectively improved MMP, as reflected by the increased TMRE fluorescence intensity. Similarly, LMWC/Ru-Cur treatment also effectively improved the MMP in Cis-induced HK-2 cells (Figure S16).

Cytochrome c (Cyt c) is a key component of mitochondrial electron transport chain complexes III and IV. High ROS levels damage the mitochondrial inner membrane, leading to Cyt c release and initiating apoptosis. ROS also triggers increased expression of BAX, which migrates to the mitochondrial membrane, further disrupting it, forming a ROS-BAX -mitochondrial damage-Cyt c release-apoptosis cycle. LMWC/Ru-Cur effectively inhibited this cycle via affecting mitochondria. Immunofluorescence results showed that oxidative stress damage induced the release of Cyt c from mitochondria to cytoplasm, as reflected by the reduced colocalization parameter (Pearson's R value). After treated with LMWC/Ru-Cur, the leakage of Cyt c was obviously reduced in HK-2 cells (Figure 5C). Immunofluorescence analysis of Bax expression revealed that LMWC/Ru-Cur effectively reduced the expression of Bax in the oxidative stress-damaged HK-2 cells (Figure 5D). In addition, immunoblotting analysis further confirmed the reduction of Bax expression following LMWC/Ru-Cur treatment. Densitometric analysis of the Western blots indicated a significant decrease in Bax protein levels in H_2O_2-treated HK-2 cells post-treatment with LMWC/Ru-Cur, compared to untreated cells (Figure 5E and F). Furthermore, the TUNEL assay confirmed that LMWC/Ru-Cur significantly decreased apoptosis in H_2O_2-induced HK-2 cells, as reflected by the reduced positive TUNEL ratio (Figure 5G and H). Overall, these results demonstrate that LMWC/Ru-Cur not only scavenges ROS but also protects mitochondrial integrity and function, thereby inhibiting the apoptotic pathways triggered by oxidative stress.

LMWC/Ru-Cur Nanodots Improved Kidney Function in AKI Mice

In vitro studies demonstrated that LMWC/Ru-Cur effectively mitigates H_2O_2-induced oxidative stress. To further validate its therapeutic efficacy, IR-AKI mice was established using Balb/c mice subjected to ischemia-reperfusion (Figure 6A). Blood creatinine (CRE) and blood urea nitrogen (BUN) levels were measured to assess kidney function. Compared to the sham group, while the IR-AKI group exhibited elevated levels in CRE and BUN. After treated with Cur, Ru-Cur, or LMWC/Ru-Cur, the CRE and BUN levels were reduced to different extent, and LMWC/Ru-Cur treatment had the better performance than Cur or Ru-Cur (Figure 6B and C). H&E staining of kidney tissues revealed that LMWC/Ru-Cur treatment effectively ameliorated ischemia-reperfusion-induced tubular damage, including brush border loss, tubular casts, and tubular epithelial cell nuclear condensation and loss (Figure 6D). The levels of SOD (Figure 6E) and MDA (Figure 6F) were significantly improved in IR-AKI mice treated with LMWC/Ru-Cur compared to those treated with Cur or Ru-Cur. Inflammatory cytokine levels were also notably reduced in IR-AKI mice treated with LMWC/Ru-

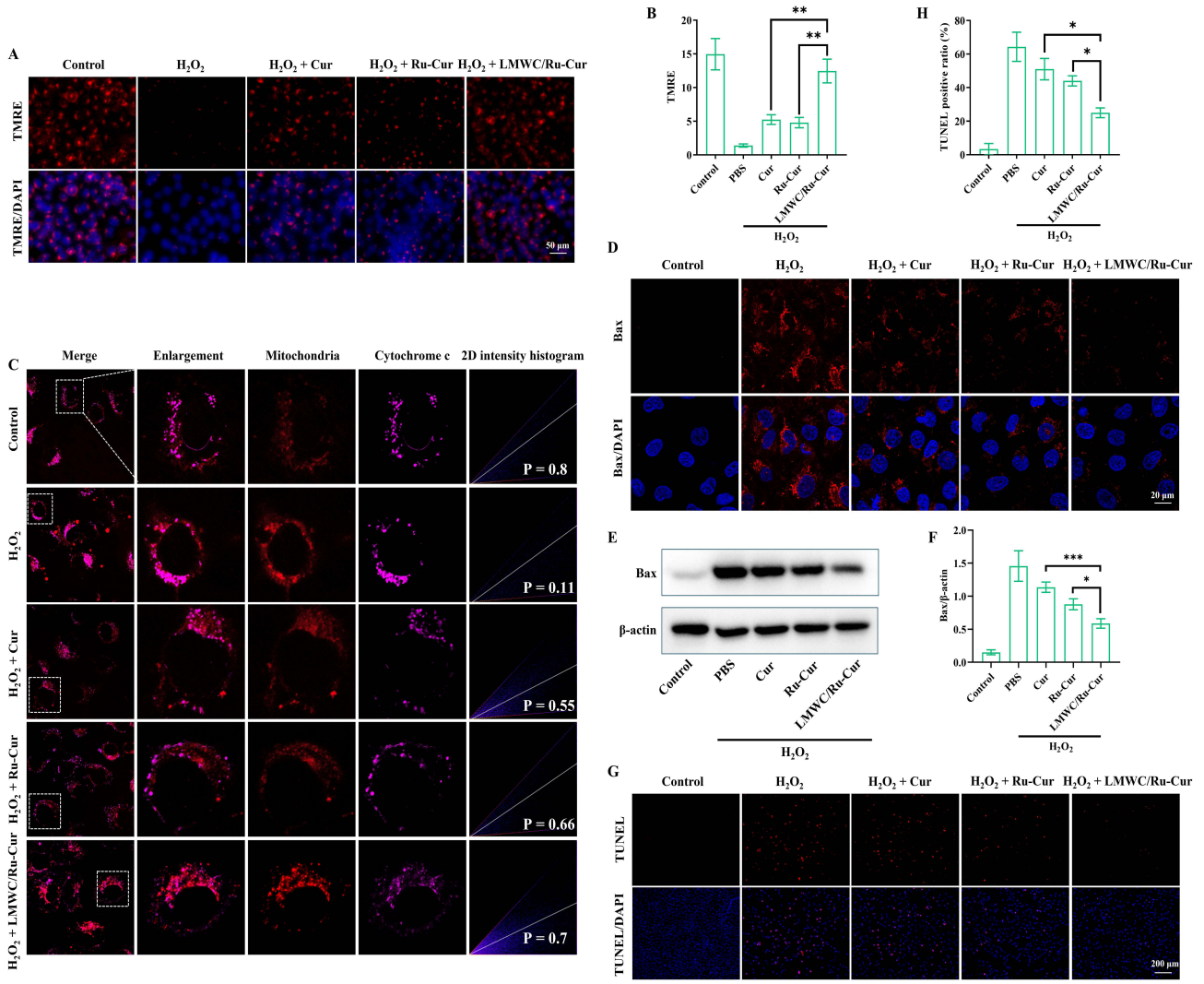

Figure 5 LMWC/Ru-Cur nanodots alleviate cell apoptosis and mitochondrial dysfunction in H_2O_2-induced HK-2 cells. (**A**) Fluorescence images of mitochondrial membrane potential in H_2O_2-induced HK-2 cells detected by TMRE probe, and (**B**) fluorescence quantitative analysis. Scale bar 50 μm. (**C**) Fluorescence images of mitochondria and Cytochrome c, and their colocalization parameter. The white dotted boxes indicate the magnified regions. (**D**) Immunofluorescence analysis on Bax expression in H_2O_2-induced HK-2 cells. Scale bar 20 μm. (**E**) Immunoblotting analysis on Bax expression in H_2O_2-induced HK-2 cells, and (**F**) densitometric analysis. (**G**) Fluorescence images of TUNEL in H_2O_2-induced HK-2 cells, and (**H**) TUNEL positive ratio. Scale bar 200 μm. Data are presented as means ± SD with n = 3 replicates per group. *p < 0.05, **p < 0.01, and ***p < 0.001.

Cur, with TNF-α (Figure 6G), and IL-6 (Figure 6H) showing significant decreases compared to both the Cur and Ru-Cur groups. As shown in Figure 6I, the fluorescence intensity of KIM-1 was significantly increased in IR-AKI mice. After treated with Cur, Ru-Cur, or LMWC/Ru-Cur, the expressions were reduced to different extent, and LMWC/Ru-Cur treatment had the best performance, as reflected by the lowest KIM-1 positive fluorescent signal. The therapeutical effect of LMWC/Ru-Cur was also examined in Cis-AKI. Similarly, LMWC/Ru-Cur treatment effectively ameliorated kidney function (CRE and BUN, Figure S17), histopathological progress (Figure S18), and KIM-1 expression (Figure S19).

The Biocompatibility of LMWC/Ru-Cur Nanodots

After incubating red blood cells with varying concentrations of LMWC/Ru-Cur for 2 h, the samples were centrifuged, and the color and clarity of the supernatant were observed to calculate hemolysis rates (Figure S20). The negative control, incubated with PBS, had a clear and transparent supernatant. Similarly, samples incubated with different concentrations of LMWC/Ru-Cur showed clear supernatants with red blood cell sedimentation. Even at a concentration of 2.0 mg/mL, the hemolysis rate of LMWC/Ru-Cur was less than 5%, indicating excellent biocompatibility.

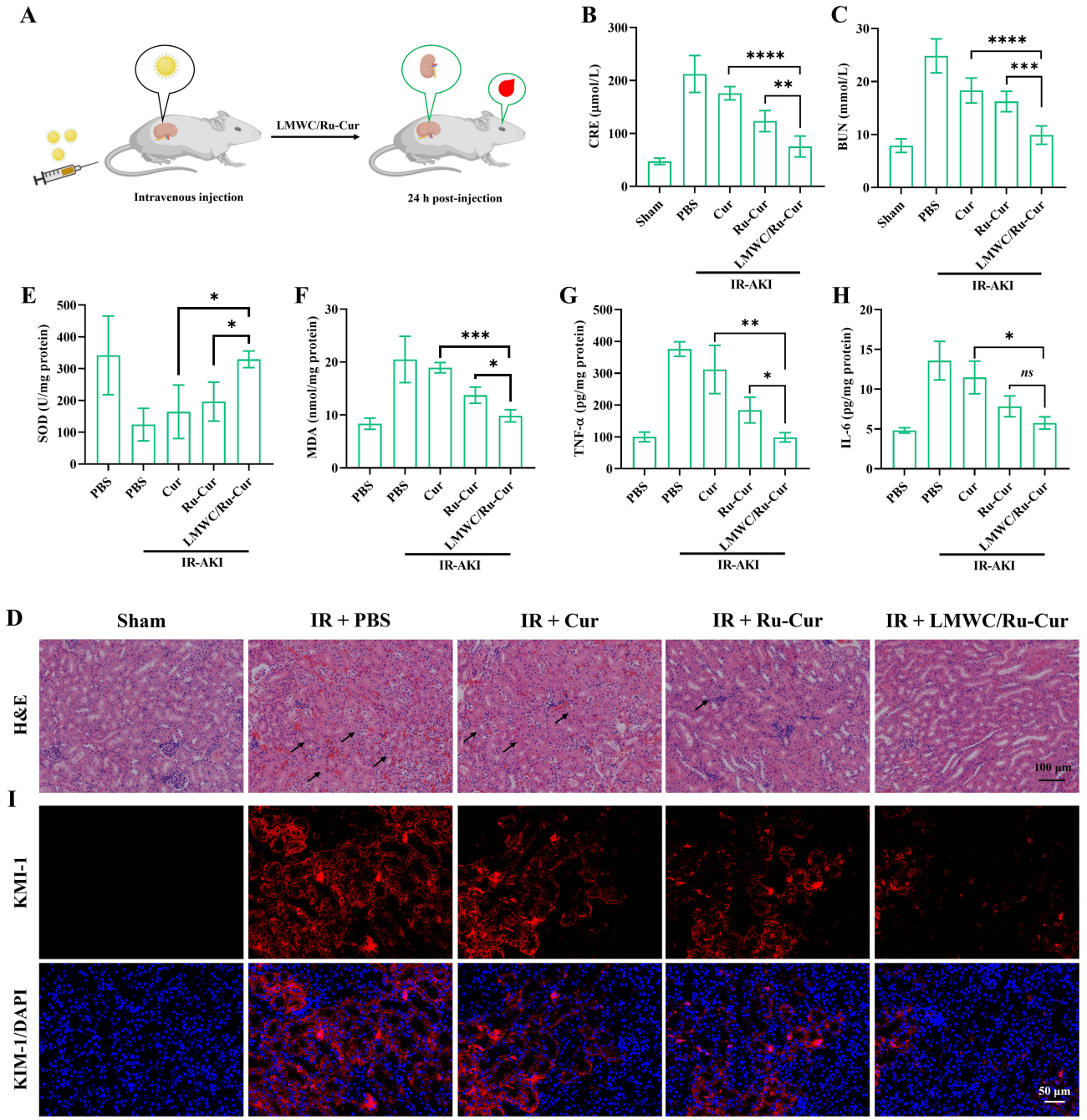

Figure 6 LMWC/Ru-Cur nanodots restore renal function and mitigate tissue damage in the IR-AKI mouse model. (**A**) Schematic diagram of treatment schedule, and therapy assessments. Renal function markers indicating the changes of (**B**) serum creatinine (CRE) and (**C**) blood urea nitrogen (BUN) levels. (**D**) Representative H&E staining sections showing the histological amelioration of kidney tissues. Black arrows indicate typical ischemia-reperfusion-induced tubular damage, including brush border loss, tubular casts, and tubular epithelial cell nuclear condensation and loss. Scale bar 100 μm. Oxidative stress and inflammatory markers in renal tissues: (**E**) SOD levels, (**F**) MDA levels, (**G**) Tumor necrosis factor-alpha (TNF-α) levels, and (**H**) Interleukin-6 (IL-6) levels. (**I**) Immunofluorescence analysis on KIM-1 expression in kidney tissues of IR-AKI mice. Scale bar 100 μm. Data are presented as means ± SD with n = 6 replicates per group. *p < 0.05, **p < 0.01, ***p < 0.001, ****p < 0.0001.
Abbreviation: ns, not significant.

There were no significant differences in RBC, WBC, PLT, lymphocytes, HGB, MCH, and MCHC levels between the blank and LMWC/Ru-Cur-treated groups at all time points (Figure S21). These findings suggested that LMWC/Ru-Cur did not cause any noticeable hematological toxicity up to 28 days post-administration. All measured parameters remained within the normal physiological range, indicating that the LMWC/Ru-Cur formulation did not induce adverse effects on blood cells. The liver and kidney function results showed no significant differences in ALT, AST, BUN, and CRE levels

https://doi.org/10.2147/IJN.S601940

between the blank and LMWC/Ru-Cur groups at any time point (Figure S22). This suggested that LMWC/Ru-Cur did not induce hepatic or renal toxicity, as all values remained within the normal range throughout the study. The absence of elevated ALT and AST levels indicated that LMWC/Ru-Cur did not cause liver damage, while normal BUN and CRE levels imply preserved kidney function.

To assess the biosafety of LMWC/Ru-Cur with respect to major organs, we conducted histological analyses. Histological examination using H&E staining at these time points revealed no significant damage in the organs (Figure S23), indicating that LMWC/Ru-Cur exhibits favorable in vivo compatibility. The observed biocompatibility supports the potential for LMWC/Ru-Cur to be effectively utilized in the treatment of AKI.

Discussion

AKI is widely recognized as a significant risk factor for the onset and progression of chronic kidney disease. Even mild AKI can lead to adverse outcomes and may progress to renal fibrosis. However, current clinical treatments for AKI are limited, highlighting an urgent need for effective therapeutic options. Mitochondrial dysfunction plays a critical role in the pathogenesis of AKI, with mitochondria being the primary source of ROS in this condition. Consequently, targeting mitochondria in the renal tubular epithelial cell is considered a promising therapeutic strategy for the treatment of AKI.[28] Nonetheless, most antioxidant strategies result in nanodrugs that are too large to pass through the glomerular system and reach the renal tubules. Therefore, this study employs ultra-small antioxidant nanodrugs, LMWC/Ru-Cur, for active renal tubular epithelial cell targeting to treat AKI.

This study successfully developed an LMWC/Ru-Cur nanodrug that combines renal targeting with efficient antioxidant functionality. The core innovation of this work lies in the integration of a dual-targeting mechanism (passive and active) and a metal-polyphenol synergistic antioxidant system. The selection of LMWC with a specific molecular weight of approximately 1500 Da and a high deacetylation degree (≥90%) was strategically determined to optimize this renal targeting. Firstly, LMWC modification enabled specific renal accumulation through size-dependent glomerular filtration and Megalin receptor-mediated endocytosis (co-localization coefficient increased 2.8-fold compared to Ru-Cur). Morphologically, this low molecular weight ensures that the functionalized nanodots stay well within the renal filtration threshold (~5.5 nm for rapid clearance in healthy state, and adaptable for injury models), facilitating their efficient passage through the glomerular barrier and subsequent accumulation in the kidney. This strategy facilitated the selective enrichment of the nanodrug in renal tubular epithelial cells, with a kidney accumulation of LMWC/Ru-Cur in the IR-AKI model being greater than that of free Cur. The clinical translation of Cur exerts significant challenges primarily due to its poor oral bioavailability and rapid systemic metabolism. Previous studies have demonstrated that Cur undergoes extensive first-pass metabolism in the liver and intestine, quickly converting into inactive metabolites such as curcumin-glucuronide and curcumin-sulfate.[29,30] This rapid metabolic clearance often results in insufficient drug concentration at the target site. Our LMWC/Ru-Cur nanodots overcome these metabolic hurdles by utilizing the LMWC-mediated renal targeting strategy. By directing the Cur specifically to the renal tubular epithelial cells via Megalin receptors, the nanoplatform not only circumvents excessive systemic metabolism but also ensures the sustained presence of active Cur at the site of AKI, thereby maximizing its therapeutic efficacy. This approach overcame the challenges traditionally faced by nanodrugs, such as size limitations preventing glomerular filtration or the rapid clearance due to the lack of targeting ligands. Secondly, the design of LMWC/Ru-Cur effectively enhanced the solubility and dispersion of Cur, significantly improving its ROS scavenging capacity. This enhancement was shown to effectively block the ROS-Bax-mitochondrial damage cascade induced by cisplatin. The design provides a paradigm for the development of metal-natural product synergistic targeted nanodrugs.

Through validation in both IR-AKI and Cis-AKI models, this study reveals the broad-spectrum therapeutic potential of LMWC/Ru-Cur. In the IR-AKI model, treatment with LMWC/Ru-Cur resulted in a 45% reduction in CRE and a 38% reduction in BUN, significantly outperforming Ru-Cur (28%/25%) and Cur (15%/12%). Furthermore, the renal tissue SOD activity was restored to 85% of normal levels, while MDA content decreased by 62%. Additionally, KIM-1 immunofluorescence showed a 73% reduction in fluorescence intensity in the LMWC/Ru-Cur group compared to the injury model, indicating its effective inhibition of renal tubular injury marker expression. Consistency across multiple models confirmed that LMWC/Ru-Cur, through its targeted delivery, ROS scavenging, and anti-apoptotic pathways, exerts synergistic effects to adapt to the complex pathological environment of AKI caused by different etiologies. This

broad-spectrum capability is particularly important for the clinical treatment of AKI, as approximately 40% of AKI cases are of unknown or multifactorial etiology.[31]

Compared to conventional antioxidant therapies, LMWC/Ru-Cur demonstrates significant advantages. It has been widely reported that nanocurcumin exhibits superior antioxidant effects, enhanced mitochondrial protection, and improved free radical scavenging capacity compared to free curcumin, largely due to its increased bioavailability. In this study, we developed LMWC/Ru-Cur nanodots as an advanced nano-delivery platform. Unlike conventional nanocurcumin, which typically relies on physical encapsulation or bulkier carriers, our LMWC/Ru-Cur nanodots leverage the structural coordination and the kidney-targeting properties of LMWC. The low molecular weight chitosan (LMWC) serves as an essential functional ligand that facilitates the specific uptake by HK-2 cells, potentially through megalin-mediated endocytosis. Our experimental data consistently demonstrated that LMWC/Ru-Cur outperformed free Cur in scavenging mitochondrial ROS, restoring SOD activity, and inhibiting lipid peroxidation (MDA levels). These results underscore that the unique nanodot architecture not only overcomes the inherent solubility limitations of curcumin but also maximizes its therapeutic efficacy in alleviating oxidative stress and protecting mitochondrial integrity in the context of AKI. Specifically, when compared to other non-targeted antioxidants, its renal targeting efficiency is 10 times greater than that of free Cur, while clinical antioxidants such as N-acetylcysteine (NAC) require high doses due to the lack of targeting ability. Secondly, the ROS scavenging capacity of LMWC/Ru-Cur exceeds that of Cur, and it specifically neutralizes mitochondrial-derived O_2^- (68% reduction in MitoSOX fluorescence intensity), whereas traditional antioxidants, such as vitamin E, only act on lipid peroxidation. In the 15 mg/kg cisplatin-induced AKI model, this nanodrug restored serum creatinine (SCr) to 89% of baseline levels, whereas the commonly used clinical agent amifostine only partially alleviates cisplatin nephrotoxicity and interferes with chemotherapy efficacy.[32] These data indicate that LMWC/Ru-Cur holds significant clinical translational potential in balancing therapeutic efficacy and safety.

Despite the significant advancements made in this study, several limitations remain. Firstly, while our in vitro data, including Megalin colocalization and competitive inhibition assays, provide compelling evidence for receptor-mediated internalization, it is important to acknowledge that the enhanced renal accumulation of LMWC/Ru-Cur in vivo may be a multifactorial outcome. Apart from active targeting, LMWC functionalization might simultaneously alter the blood circulation half-life and glomerular filtration kinetics, thereby contributing to the overall increase in renal deposition. Furthermore, it is unclear whether LMWC interacts with other high-expression receptors in the renal tubules. Due to the lack of causal verification via conditional Megalin gene knockout or direct pharmacological inhibition models (eg, Receptor-Associated Protein (RAP) or specific siRNA) in the current study, the precise mechanistic attribution between active targeting and altered pharmacokinetics remains to be fully elucidated. This limitation will be addressed in future studies using more stringent genetic or pharmacological validation to rigorously establish the causality of the targeting mechanism. Secondly, although LMWC/Ru-Cur exhibited no toxicity in the 28-day biocompatibility study (hemolysis rate <5%, with normal liver and kidney function markers), its long-term metabolic pathways-particularly the potential risk of extra-renal accumulation of Ru ions-require further evaluation using isotope tracing techniques. Additionally, this study did not investigate the efficacy of the nanodrug in a chronic kidney disease (CKD)-induced AKI model, where the decline in glomerular filtration rate in CKD patients may affect passive targeting efficiency. Furthermore, although LMWC/Ru-Cur achieved promising therapeutic efficacy at a low Cur-equivalent dose (2 mg/kg) compared to traditional high-dose free Cur treatments, comprehensive dose-escalation and toxicity studies were not conducted in the present study. Future preclinical evaluations are imperative to fully decipher its precise therapeutic window, lowest effective concentration, and maximal tolerated dose (MTD) before moving toward clinical translation. Future work could focus on the following directions: ① exploring the synergistic effects of LMWC/Ru-Cur in combination with existing chemotherapy regimens (such as cisplatin); ② employing single-cell sequencing technology to analyze the targeting preference of the nanodrug for different renal tubular cell subpopulations. These improvements will help advance this nanoplatform toward personalized treatment for AKI.

While our current IR and cisplatin-induced models successfully demonstrate the efficacy of LMWC/Ru-Cur in mitigating localized oxidative stress, we acknowledge that these models may not fully translate to other major clinical categories such as sepsis-associated AKI (SA-AKI).[33] SA-AKI is primarily driven by systemic inflammation and hemodynamic instability rather than isolated localized oxidative stress. Consequently, it remains to be further investigated whether a purely ROS-scavenging mechanism is sufficient for SA-AKI, where profound systemic inflammation is the predominant injury driver. Furthermore,

regarding the potential to prevent the progression from AKI to CKD,[34] our current acute-phase data, including the significant reduction of pro-inflammatory cytokines (such as TNF-α and IL-6), only provide correlative evidence. Direct proof demonstrating that this acute ROS-scavenging intervention definitively prevents long-term fibrosis warrants extended long-term follow-up studies in the future.

Conclusion

In conclusion, this study demonstrated that LMWC/Ru-Cur nanodots provided a promising therapeutic strategy for acute kidney injury. By effectively scavenging reactive oxygen species and reducing mitochondrial damage, the nanodots significantly improved renal function, mitigated oxidative stress, and reduced inflammation in both cellular and animal models of acute kidney injury induced by ischemia-reperfusion or cisplatin. These results highlighted the potential of LMWC/Ru-Cur nanodots to serve as a novel treatment approach, offering enhanced protection against acute kidney injury through reactive oxygen species scavenging and the preservation of mitochondrial function.

Data Sharing Statement

All data supporting the findings of this study are available from the corresponding author (Qin Yu, 454699984@qq.com) upon reasonable request.

Ethics Approval and Consent to Participate

Balb/c mice (equal numbers of males and females; 22–25 g) were purchased from SpePharm (Beijing) Biotechnology Co., Ltd. All procedures complied with the ARRIVE guidelines and the U.S. National Institutes of Health standards for the ethical care and use of laboratory animals. Experiments were approved by the Animal and Medical Ethics Committee of Zhejiang Huitong Test & Evaluation Technology Group Co., Ltd. (approval no. HT-2024-LWFB-0004).

Funding

This research was funded by the Nature Science Foundation of Zhejiang province (LGF22H090023), Ningbo City Health and Wellness Technology Program (2024Y41), and Beilun District health science and technology project (2024BLWSQN006, 2025BLWSQN013).

Disclosure

The authors declare no competing interests.

References

1. Muruve DA. Inflammasomes and acute kidney injury. *J Am Soc Nephrol*. 2024;35(8):985–987. doi:10.1681/ASN.0000000000000423
2. Legrand M, Clark AT, Neyra JA, Ostermann M. Acute kidney injury in patients with burns. *Nat Rev Nephrol*. 2024;20(3):188–200. doi:10.1038/s41581-023-00769-y
3. Cullis B, McCulloch M, Finkelstein FO. Development of PD in lower-income countries: a rational solution for the management of AKI and ESKD. *Kidney Int*. 2024;105(5):953–959. doi:10.1016/j.kint.2023.11.036
4. Hirsch JS, Ng JH, Ross DW, et al. Acute kidney injury in patients hospitalized with COVID-19. *Kidney Int*. 2020;98(1):209–218. doi:10.1016/j.kint.2020.05.006
5. Chen HC, Hou HY, Sung JM, Shieh CC. Deletion of NADPH oxidase 2 attenuates cisplatin-induced acute kidney injury through reducing ROS-induced proximal tubular cell injury and inflammation. *Front Med*. 2023;10:1097671. doi:10.3389/fmed.2023.1097671
6. Ma Y, Cai F, Li Y, Chen J, Han F. Lin W: a review of the application of nanoparticles in the diagnosis and treatment of chronic kidney disease. *Bioact Mater*. 2020;5(3):732–743. doi:10.1016/j.bioactmat.2020.05.002
7. Wang Y, Zhao S, Ni N, et al. Nanoparticles induced glomerular endothelial leakiness promoting albuminuria level. *NanoImpact*. 2025;37:100548. doi:10.1016/j.impact.2025.100548
8. Liu X, Yu Q, Mao HB, Hu JB, Liu WH. Ultra-small curcumin-ruthenium coordination polymer nanodots prevent renal ischemia-reperfusion injury and the progression to chronic kidney disease. *Front Bioeng Biotechnol*. 2024;12:1506909. doi:10.3389/fbioe.2024.1506909
9. Wang DW, Li SJ, Tan XY, et al. Engineering of stepwise-targeting chitosan oligosaccharide conjugate for the treatment of acute kidney injury. *Carbohydr Polym*. 2021;256:117556. doi:10.1016/j.carbpol.2020.117556
10. Funahashi Y, Park SH, Hebert JF, et al. Nanotherapeutic kidney cell-specific targeting to ameliorate acute kidney injury. *Kidney Int*. 2024;106(4):597–610. doi:10.1016/j.kint.2024.06.021
11. Mhaidat I, Alwedian F, Ababneh T, Shdefat A, Tashtoush H. Synthesis, characterization, computational, antioxidant and fluorescence properties of novel 1,3,5-trimesic hydrazones derivatives. *Heliyon*. 2021;7(9):e08074. doi:10.1016/j.heliyon.2021.e08074

12. Vahdati SN, Lashkari A, Navasatli SA, Ardestani SK, Safavi M. Butylated hydroxyl-toluene, 2,4-Di-tert-butylphenol, and phytol of Chlorella sp. protect the PC12 cell line against H(2)O(2)-induced neurotoxicity. *Biomed Pharmacother*. 2022;145:112415. doi:10.1016/j.biopha.2021.112415
13. He Z, Liu Y, Wang H, et al. Dual-grafted dextran based nanomicelles: higher antioxidant, anti-inflammatory and cellular uptake efficiency for quercetin. *Int J Biol Macromol*. 2023;224:1361–1372. doi:10.1016/j.ijbiomac.2022.10.222
14. Ghani AA, Devarayapalli KC, Kim B, et al. Sodium-alginate-laden MXene and MOF systems and their composite hydrogel beads for batch and fixed-bed adsorption of naproxen with electrochemical regeneration. *Carbohydr Polym*. 2023;318:121098. doi:10.1016/j.carbpol.2023.121098
15. Zhou LB, Peng XZ, Long HM, Hu JB, Xu JT. Stepwise targeting hyaluronic acid-based polymeric prodrug for acute kidney injury and prevents its progression to chronic kidney disease. *Mater Today Bio*. 2025;34:102207. doi:10.1016/j.mtbio.2025.102207
16. Mora FAA, Musheshe N, Arroyave Ospina JC, et al. Metformin protects against diclofenac-induced toxicity in primary rat hepatocytes by preserving mitochondrial integrity via a pathway involving EPAC. *Biomed Pharmacother*. 2021;143:112072. doi:10.1016/j.biopha.2021.112072
17. Ajibare AC, Ebuehi OAT, Adisa RA, et al. Fractions of Hoslundia opposita Vahl and hoslundin induced apoptosis in human cancer cells via mitochondrial-dependent reactive oxygen species (ROS) generation. *Biomed Pharmacother*. 2022;153:113475. doi:10.1016/j.biopha.2022.113475
18. Li N, Zhang G, Chen Y, et al. Identification of the mimotopes within the major capsid protein L1 of human papillomavirus types 18 and 45, using neutralizing monoclonal antibodies. *Int J Biol Macromol*. 2021;174:587–595. doi:10.1016/j.ijbiomac.2021.01.137
19. Gillis EE, Brands MW, Sullivan JC. Adverse maternal and fetal outcomes in a novel experimental model of pregnancy after recovery from renal ischemia-reperfusion injury. *J Am Soc Nephrol*. 2021;32(2):375–384. doi:10.1681/ASN.2020020127
20. Yao X, Zhang Y, Zhang B, Deng Z, Li H. The structure change of polygonatum polysaccharide and the protect effect of Polygonatum crtonema Hua extracts and polysaccharide on cisplatin-induced AKI mice during nine-steam-nine-bask processing. *Int J Biol Macromol*. 2024;277(Pt 2):132290. doi:10.1016/j.ijbiomac.2024.132290
21. Cai Y, Xin L, Sun P, Li H, Liu C, Fang L. Temperature-sensitive multifunctional intelligent responsive hydrogel based on carboxymethyl agarose and N-isopropylacrylamide: controlled drug release and accelerated wound healing. *Carbohydr Polym*. 2023;322:121327. doi:10.1016/j.carbpol.2023.121327
22. Shen P, Huang K, Zhang X, et al. Genetically engineered MSC-derived hybrid cellular vesicles for ROS-scavenging and mitochondrial homeostasis in hepatic ischemia-reperfusion injury. *Mater Today Bio*. 2025;34:102215. doi:10.1016/j.mtbio.2025.102215
23. Li YX, Bao YT, Hu JB. Engineering of targeting antioxidant polypeptide nanopolyplexes for the treatment of acute lung injury. *Int J Biol Macromol*. 2024;254(Pt 3):127872. doi:10.1016/j.ijbiomac.2023.127872
24. Li Y, Hou H, Liu Z, et al. CD44 targeting nanodrug based on chondroitin sulfate for melanoma therapy by inducing mitochondrial apoptosis pathways. *Carbohydr Polym*. 2023;320:121255. doi:10.1016/j.carbpol.2023.121255
25. Lv J, Li Y, Shi S, et al. Skeletal muscle mitochondrial remodeling in heart failure: an update on mechanisms and therapeutic opportunities. *Biomed Pharmacother*. 2022;155:113833. doi:10.1016/j.biopha.2022.113833
26. Cai J, Jiao X, Luo W, et al. Kidney injury molecule-1 expression predicts structural damage and outcome in histological acute tubular injury. *Ren Fail*. 2019;41(1):80–87. doi:10.1080/0886022X.2019.1578234
27. Qu M, Ni Y, Guo B, Feng X, Jiang Z. Lycopene antagonizes lead toxicity by reducing mitochondrial oxidative damage and mitochondria-mediated apoptosis in cultured hippocampal neurons. *MedComm*. 2020;1(2):228–239. doi:10.1002/mco2.17
28. Chen Y, Li Z, Zhang H, et al. Mitochondrial metabolism and targeted treatment strategies in ischemic-induced acute kidney injury. *Cell Death Discov*. 2024;10(1):69. doi:10.1038/s41420-024-01843-5
29. Vareed SK, Kakarala M, Ruffin MT, et al. Pharmacokinetics of curcumin conjugate metabolites in healthy human subjects. *Cancer Epidemiol Biomarkers Prevention*. 2008;17(6):1411–1417. doi:10.1158/1055-9965.EPI-07-2693
30. Anand P, Kunnumakkara AB, Newman RA, Aggarwal BB. Bioavailability of curcumin: problems and promises. *Mol Pharmaceut*. 2007;4(6):807–818. doi:10.1021/mp700113r
31. Legrand M, Bagshaw SM, Bhatraju PK, et al. Sepsis-associated acute kidney injury: recent advances in enrichment strategies, sub-phenotyping and clinical trials. *Crit Care*. 2024;28(1):92. doi:10.1186/s13054-024-04877-4
32. Duan Z, Cai G, Li J, Chen X. Cisplatin-induced renal toxicity in elderly people. *Ther Adv Med Oncol*. 2020;12:1758835920923430. doi:10.1177/1758835920923430
33. Wang L, Li ZY, Zhong CL, et al. Therapeutic potential of naturally derived carbon dots in sepsis-associated acute kidney injury. *Chin Med*. 2025;20:49. doi:10.1186/s13020-025-01103-3
34. Liu T, Wu Y, Wang C, et al. Mulberry-derived carbon dots attenuate kidney fibrosis through direct inhibition of PI3K. *Mater Today Bio*. 2025;35:102626. doi:10.1016/j.mtbio.2025.102626